

## RESEARCH ARTICLE

## Dowker complex based machine learning (DCML) models for protein-ligand binding affinity prediction

Xiang Liu<sup>1,2,3</sup>, Huitao Feng<sup>2,4</sup>, Jie Wu<sup>3,5</sup>, Kelin Xia<sup>1\*</sup>

**1** Division of Mathematical Sciences, School of Physical and Mathematical Sciences, Nanyang Technological University, Singapore, **2** Chern Institute of Mathematics and LPMC, Nankai University, Tianjin, China, **3** Center for Topology and Geometry Based Technology, Hebei Normal University, Hebei, China, **4** Mathematical Science Research Center, Chongqing University of Technology, Chongqing, China, **5** School of Mathematical Sciences, Hebei Normal University, Hebei, China

\* [xiakelin@ntu.edu.sg](mailto:xiakelin@ntu.edu.sg)

## OPEN ACCESS

**Citation:** Liu X, Feng H, Wu J, Xia K (2022) Dowker complex based machine learning (DCML) models for protein-ligand binding affinity prediction. *PLoS Comput Biol* 18(4): e1009943. <https://doi.org/10.1371/journal.pcbi.1009943>

**Editor:** Joanna Slusky, University of Kansas, UNITED STATES

**Received:** September 14, 2021

**Accepted:** February 21, 2022

**Published:** April 6, 2022

**Peer Review History:** PLOS recognizes the benefits of transparency in the peer review process; therefore, we enable the publication of all of the content of peer review and author responses alongside final, published articles. The editorial history of this article is available here: <https://doi.org/10.1371/journal.pcbi.1009943>

**Copyright:** © 2022 Liu et al. This is an open access article distributed under the terms of the [Creative Commons Attribution License](https://creativecommons.org/licenses/by/4.0/), which permits unrestricted use, distribution, and reproduction in any medium, provided the original author and source are credited.

**Data Availability Statement:** The PDBbind datasets are available at <http://www.pdbbind.org.cn/>, and the code is available on GitHub at <https://github.com/LiuXiangMath/Dowker-Complex-Based-ML>.

## Abstract

With the great advancements in experimental data, computational power and learning algorithms, artificial intelligence (AI) based drug design has begun to gain momentum recently. AI-based drug design has great promise to revolutionize pharmaceutical industries by significantly reducing the time and cost in drug discovery processes. However, a major issue remains for all AI-based learning model that is efficient molecular representations. Here we propose Dowker complex (DC) based molecular interaction representations and Riemann Zeta function based molecular featurization, for the first time. Molecular interactions between proteins and ligands (or others) are modeled as Dowker complexes. A multiscale representation is generated by using a filtration process, during which a series of DCs are generated at different scales. Combinatorial (Hodge) Laplacian matrices are constructed from these DCs, and the Riemann zeta functions from their spectral information can be used as molecular descriptors. To validate our models, we consider protein-ligand binding affinity prediction. Our DC-based machine learning (DCML) models, in particular, DC-based gradient boosting tree (DC-GBT), are tested on three most-commonly used datasets, i.e., including PDBbind-2007, PDBbind-2013 and PDBbind-2016, and extensively compared with other existing state-of-the-art models. It has been found that our DC-based descriptors can achieve the state-of-the-art results and have better performance than all machine learning models with traditional molecular descriptors. Our Dowker complex based machine learning models can be used in other tasks in AI-based drug design and molecular data analysis.

## Author summary

With the ever-increasing accumulation of chemical and biomolecular data, data-driven artificial intelligence (AI) models will usher in an era of faster, cheaper and more-efficient drug design and drug discovery. However, unlike image, text, video, audio data, molecular

**Funding:** This work was supported in part by Nanyang Technological University Startup Grant M4081842 and Singapore Ministry of Education Academic Research fund Tier 1 RG109/19, MOE-T2EP20120-0013 and MOE-T2EP20220-0010. The first author (XL) was supported by Nankai Zhide foundation. The second author (HF) was supported by Natural Science Foundation of China (NSFC grant no. 11931007, 11221091, 11271062, 11571184). The third author (JW) was supported by Natural Science Foundation of China (NSFC grant no. 11971144) and High-level Scientific Research Foundation of Hebei Province. The funders had no role in study design, data collection and analysis, decision to publish, or preparation of the manuscript.

**Competing interests:** The authors have declared that no competing interests exist.

data from chemistry and biology, have much complicated three-dimensional structures, as well as physical and chemical properties. Efficient molecular representations and descriptors are key to the success of machine learning models in drug design. Here, we propose Dowker complex based molecular representation and Riemann Zeta function based molecular featurization, for the first time. To characterize the complicated molecular structures and interactions at the atomic level, Dowker complexes are constructed. Based on them, intrinsic mathematical invariants are derived and used as molecular descriptors, which can be further combined with machine learning and deep learning models. Our model has achieved state-of-the-art results in protein-ligand binding affinity prediction, demonstrating its great potential for other drug design and discovery problems.

## Introduction

Featurization (or feature engineering) is of essential importance for AI-based drug design. The performance of quantitative structure activity/property relationship (QSAR/QSPR) models and machine learning models for biomolecular data analysis is largely determined by the design of proper molecular descriptors/fingerprints. Currently, more than 5000 types of molecular descriptors, which are based on molecular structural, chemical, physical and biological properties, have been proposed [1, 2]. Among these molecular features, structural descriptors are the most-widely used ones and can be classified into one-dimensional (1D), two-dimensional (2D), three-dimensional (3D), and four-dimensional (4D) [1, 2]. In general, 1D molecular descriptors are atom counts, bond counts, molecular weight, fragment counts, functional group counts, and other summarized general properties. The 2D molecular descriptors are topological indices, graph properties, combinatorial properties, molecular profiles, autocorrelation coefficients, and other topological/graphic/combinatorial properties. The 3D molecular descriptors are molecular surface properties, volume properties, autocorrelation descriptors, substituent constants, quantum chemical descriptors, and other geometric or density-function related properties. The 4D chemical descriptors are usually generated from a dynamic process that covers various molecular configurations. Further, various molecular fingerprints are proposed, including substructure key based fingerprints [3], path-based fingerprints [4, 5], circular fingerprints [6], pharmacophore fingerprints [7, 8], and autoencoded fingerprints. Different from molecular descriptors, molecular fingerprint is large-sized vector of molecular features that are systematically generated based on molecular properties, in particular, structural properties. Deep learning models, such as autoencoder, CNN, and GNN, have also been used in molecular fingerprint generation [9–13].

The generalizability and transferability of QSAR/QSPR and machine learning models are highly related to molecular descriptors or fingerprints. Features that characterize more intrinsic and fundamental properties can be better shared between data and “understood” by machine learning models. Mathematical invariants, from geometry, topology, algebra, combinatorics and number theory, are highly abstract quantities that describe the most intrinsic and fundamental rules and properties in nature sciences. In particular, topological and geometric invariants based molecular descriptors have achieved great successes in various steps of drug design, including protein-ligand binding affinity prediction [14–18], protein stability change upon mutation prediction [19, 20], toxicity prediction [21], solvation free energy prediction [22, 23], partition coefficient and aqueous solubility [24], binding pocket detection [25], and drug discovery [26]. These models have also demonstrated great advantages over traditional

molecular representations in D3R Grand challenge [27–29]. Recently, persistent models, including hypergraph-based persistent homology [30, 31], persistent spectral [32], and persistent Ricci curvature [33–36], have been developed for molecular characterization and delivered great performance in protein-ligand binding affinity prediction.

Dowker complex (DC) is developed for the characterization of relations between two sets [37–39]. Mathematically, Dowker complex (DC) is defined on two sets  $X$  and  $Y$  with a relation  $R$ , which is a subset of the product set  $X \times Y$ . The elements in the same set can form a simplex in DC if they all have relation with a common element from the other set. Note that only elements in the same set, i.e., either  $X$  or  $Y$ , can form simplexes. Stated differently, a simplex in DC can never be formed among elements from both sets. In this way, a DC can be separated into two disjoint simplicial complexes, i.e., one with elements all from  $X$  and the other with elements all from  $Y$ . These two simplicial complexes share the same homology groups, homotopy groups, and homotopy types [37, 38]. Moreover, DCs are equivalent to Neighborhood complex (NC) for all bipartite graphs. In fact, if the relations between two sets are represented by a bipartite graph, its associated DC is exact the same as NC. Further, Riemann Zeta function or Euler Riemann Zeta function, is a mathematical function of a complex variable. The Riemann Zeta function plays a pivotal role in analytic number theory and has applications in physics, probability theory, and applied statistics. Mathematically, Riemann Zeta function can be used in the characterization of intrinsic information of the system.

Here we propose Dowker complex based molecular interaction representations and Riemann Zeta function based molecular featurization, for the first time. More specifically, a bipartite graph can be used to model the interactions between two molecules, such as a protein and a ligand. Mathematically, a bipartite graph can be viewed as a relation between two sets, and a Dowker complex can be generated naturally from it. Further, a DC has two disjoint components, which share the same homology groups. For a protein-ligand complex, protein-based DC and ligand-based DC have the same Betti number. Further, DC-based persistent spectral models can be constructed from a filtration process, and persistent Riemann Zeta functions are used as molecular descriptors or fingerprints. Our DC-based machine learning models, in particular, DC-based gradient boosting tree (DC-GBT), are extensively tested on the three most-commonly used datasets from the well-established protein-ligand binding databank of PDBbind. It is found that our DC-GBT model has achieved state-of-the-art results and are better than all machine learning models with traditional molecular descriptors.

## Results

### DC-based biomolecular interaction analysis

Molecular representation and featurization are of essential importance for the analysis of molecular data from materials, chemistry and biology. Mathematical invariant based molecular descriptors are of greater transferability thus have achieved better performance in AI-based drug design [20, 40–42]. Here we propose the first DC-based representations for molecular interaction analysis.

**Bipartite graph-based molecular interaction characterization.** Graph theory is widely used for the description and characterization of molecular structures and interactions. A molecular graph  $G = (V, E)$  is composed of a set of vertices  $V$ , with each vertex representing molecular atom, residue, motif, or even the entire molecule, and a set of edges  $E$ , representing interactions of various kinds including covalent bonds, van der Waals, electrostatic, and other non-covalent forces. Both intra- and inter- molecular interactions, i.e., interactions within and between molecules, can be represented as bipartite graphs (also known as bigraphs or 2-mode networks). Mathematically, a bipartite graph  $G(V_1, V_2, E)$  has two vertex sets  $V_1$  and  $V_2$ , and

all its edges are formed only between the two vertex sets. Recently, bipartite-graph based interactive matrixes have been used for machine learning models in drug design and achieved great success [20, 30–34, 40]. Mathematically, these interactive matrixes, which are based on atomic distances and electrostatic interactions, can be transformed into a weighted biadjacency matrixes between protein and ligand atoms. More specifically, if we let  $V_P = \{v_i | i = 0, 1, \dots, N_P\}$  and  $V_L = \{v_j | j = 0, 1, \dots, N_L\}$  represent the coordinate sets of protein and ligand atoms respectively, the biadjacency matrix  $\mathbf{B}$  with a size  $N_P \times N_L$  is defined as follows,

$$\mathbf{B}(v_i, v_j) = w_{ij}, v_i \in V_P \text{ and } v_j \in V_L. \quad (1)$$

The weights  $w_{ij}$  can be chosen as the Euclidean distances or electrostatic interactions [20]. Essentially, inter-molecular interactions between protein and ligand atoms are characterized in the above biadjacency matrix.

Two individual unipartite graphs  $G_1$  and  $G_2$  can be constructed from a bipartite graph  $G(V_1, V_2, E)$  through a projection process [43, 44]. More specifically, the unipartite graph  $G_1$  is generated from vertex set  $V_1$ , and its edges are defined between any two vertices that have a common neighborhood vertex in  $V_2$ . Similarly, the unipartite graph  $G_2$  is based on vertex set  $V_2$ , and any two vertices that have a common neighborhood vertex in  $V_1$  will form an edge in  $G_2$ . Mathematically, the connection matrixes for the unipartite graphs can be generated from the adjacency matrix as in Eq (1). The connection matrixes for protein and ligand are  $\mathbf{B}\mathbf{B}^T$  and  $\mathbf{B}^T\mathbf{B}$ , respectively. Note that the two matrixes are of different sizes. Further, based on the unipartite graphs  $G_1$  and  $G_2$ , two flag complexes (or clique complexes),  $K_{F,1}(G)$  and  $K_{F,2}(G)$  can be constructed respectively. More specifically, in the two flag complexes, a  $k$ -complex is formed among  $k + 1$  vertices when any two vertices are connected by an edge.

**Bipartite graph-based DC models.** Mathematically, a bipartite graph can be seen as a relation. Two Dowker complexes  $K_{D,1}(G)$  and  $K_{D,2}(G)$  can be naturally constructed from a bipartite graph  $G(V_1, V_2, E)$ . The DC  $K_{D,1}(G)$  is defined on  $V_1$ , and its  $k$ -simplex is formed among  $k + 1$  vertices which have “relations”, i.e., forming edges, with a common vertex in  $V_2$ . Similarly, the DC  $K_{D,2}(G)$  is based on  $V_2$ , and its  $k$ -simplex is formed among  $k + 1$  vertices which are “related to” a common vertex in  $V_1$ . Note that when vertices are related to a common vertex, that means they share the same common neighborhood vertex and a DC-based simplex will be formed among them.

Further, the Dowker theorem states that the homology of  $K_{D,1}(G)$  and  $K_{D,2}(G)$  are isomorphic, which means  $H_p(K_{D,1}(G)) \cong H_p(K_{D,2}(G)) (p > 0)$ , and 0-th homology is isomorphic if the bipartite graph  $G$  is connected [38, 39]. It is worth mentioning that the flag complexes, i.e.,  $K_{F,1}(G)$  and  $K_{F,2}(G)$ , from the unipartite graphs are usually different from the DCs. Fig 1 illustrates the bipartite graph-based DCs and their persistent barcodes. The bipartite graph is generated from the phosphorus-phosphorus (P-P) interactions between two chains from DNA 1D77. The corresponding DC has two disjoint components, one from chain A and the other from chain B. The distance-based filtration process is considered and two persistent barcodes for chain A and chain B are generated. It can be observed that  $\beta_1$  persistent barcodes are exactly the same. Note that  $\beta_0$  persistent barcodes are not the same as the bipartite graphs are not always connected during the filtration process.

## DC-based persistent spectral models

For all the persistent models, including persistent homology/cohomology, persistent spectral and persistent function, the key point is the filtration process. There are various ways to define the filtration parameter, leading to different filtration processes. For topology-based protein-ligand interaction models, we can define the filtration parameter  $f$  as the weight value of the

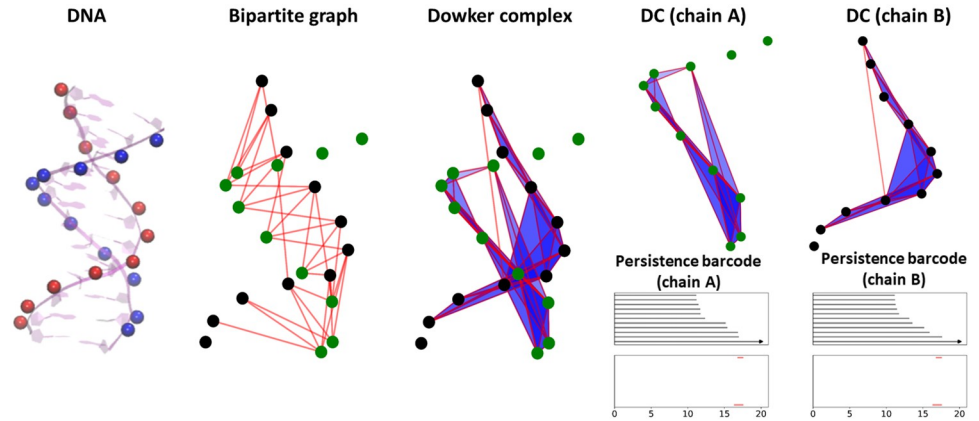


**Fig 1. Dowker complex based representation for the atomic interactions between two chains of DNA 1D77.** Only the Phosphor (P) atoms of the DNA are considered. A bipartite graph is constructed between the two DNA chains, i.e., chain A and chain B, using a cutoff distance of 16.5 Å. The corresponding Dowker complex is generated and consists of two disjoint components, one from chain A and the other from chain B. The cutoff distance can be used a filtration parameter and two persistent barcodes are obtained. It can be seen that the  $\beta_1$  persistent barcodes are exactly the same for the two types of DCs from chain A and chain B. The  $\beta_0$  persistent barcodes are different because the bipartite graph are not always connected during the filtration process.

<https://doi.org/10.1371/journal.pcbi.1009943.g001>

biadjacency matrix in Eq (1). With the increase of filtration value, a series of nested bipartite graphs can be generated,

$$G_{f_0} \subset G_{f_1} \subset \dots \subset G_{f_n}. \tag{2}$$

Here ( $f_0 \leq f_1 \leq \dots \leq f_n$ ) are filtration values. The corresponding DCs can be constructed accordingly as follows,

$$K_D(G_{f_0}) \subset K_D(G_{f_1}) \subset \dots \subset K_D(G_{f_n}). \tag{3}$$

In fact, we have two disjointed series of nested DCs as follows,

$$K_{D,1}(G_{f_0}) \subset K_{D,1}(G_{f_1}) \subset \dots \subset K_{D,1}(G_{f_n}). \tag{4}$$

$$K_{D,2}(G_{f_0}) \subset K_{D,2}(G_{f_1}) \subset \dots \subset K_{D,2}(G_{f_n}). \tag{5}$$

Note that the first DC series  $\{K_{N,1}(G_{f_i})\}$  are for protein part, all of their vertices are protein atoms. In contrast, the second DC series  $\{K_{N,2}(G_{f_i})\}$  are fully based on ligand atoms. From Dowker’s theorem, these two DC series share the same homology groups, i.e.,  $H_p(K_{D,1}(G_{f_i})) \cong H_p(K_{D,2}(G_{f_i}))$  ( $p > 0, i = 1, 2, \dots, n$ ).

Persistent spectral (PerSpect) models are proposed to study the persistence and variation of spectral information of the topological representations during a filtration process [32]. These spectral information can be used as molecular descriptors or fingerprints and combined with machine learning models for drug design. Here we study DC-bases persistent spectral models. From the Eqs (4) and (5), two sequences of Hodge Laplacian matrixes can be generated respectively (see Materials and methods). These matrixes characterize the interactions between protein and ligand atoms at various different scales. The spectral information derived from these Hodge Laplacian matrixes are used for the characterization of protein-ligand interactions. Fig 2 illustrates DC-based filtration process and the corresponding Hodge Laplacian matrixes for the protein-ligand complex 2POG. From the bipartite sequence, two separated series of DCs



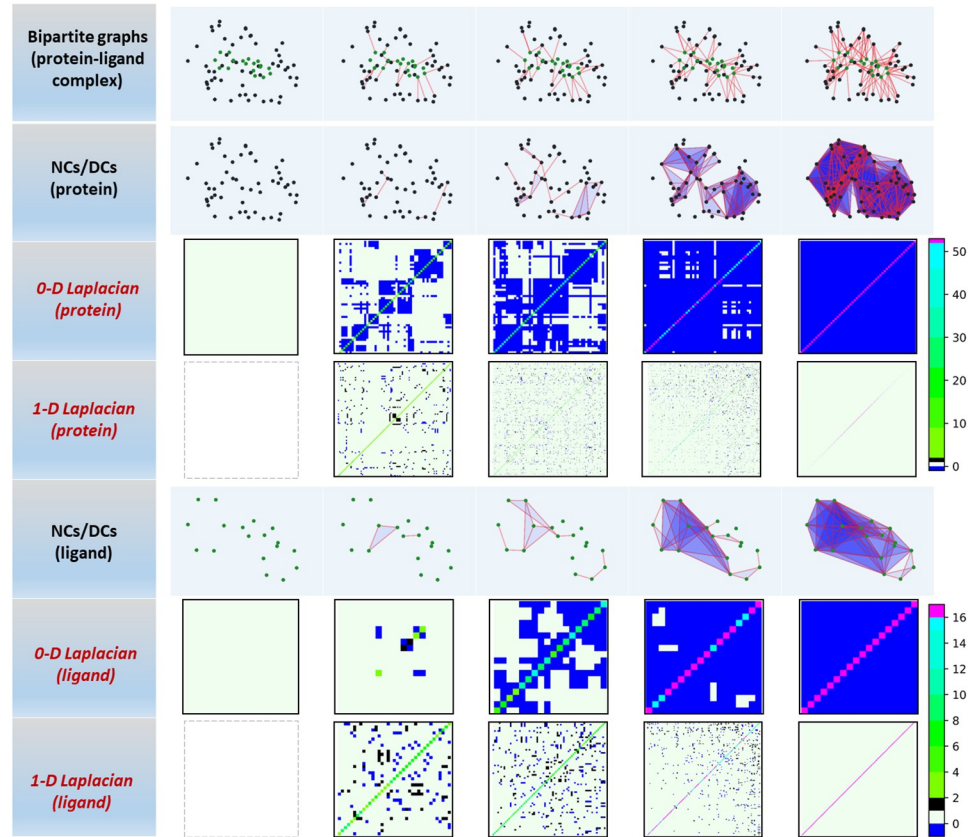


**Fig 2. Persistent combinatorial Laplacian matrixes for Dowker complex from C-C pair of PDBID 2POG.** As in the picture, based on the filtration process of bipartite graphs, a filtration of Dowker complexes can be generated and further divided into two disjoint filtration processes in protein and ligand. Then for each filtration process, two sequence of laplacian matrixes in dimension 0 and 1 are depicted. The cutoff extracting the binding core region is 5Å, filtration values are 3.5Å, 4Å, 4.2Å, 4.5Å and 5Å. For 0-D laplacian matrixes, with the increase of filtration value, the matrix size is always same, off-diagonal entries decrease from 0 to -1 until all become -1 and diagonal entries increase until all up to the number of 0-simplexes minus 1. For 1-D laplacian matrixes, the matrix size increase consistently until up to a constant, and off-diagonal entries have nonzero values 1 and -1 due to their orientation and the number of off-diagonal nonzero entries increase at early stage and then decrease until all go to zero, and diagonal entries increase until all up to the number of 0-simplexes.

<https://doi.org/10.1371/journal.pcbi.1009943.g002>

are generated based on protein atoms and ligand atoms respectively. We consider the 0-dimensional (0-D) and 1-dimensional (1-D) Hodge Laplacian matrixes. Note that 0-D Hodge Laplacian matrixes represent topological connections between vertices, while 1-D matrixes characterize topological connections between edges. Similarly, other-higher dimensional Hodge Laplacian matrixes can be generated for higher-dimensional simplexes. Further, the multiplicity of zero-eigenvalues for the  $k$ -th dimensional Hodge Laplacian matrixes is  $\beta_k$ , i.e., the  $k$ -th Betti number. Additionally, information from non-zero-eigenvalues indicates “geometric” properties of the simplicial complexes [32].

Spectral information, i.e., eigenvalues and eigenvectors, from our PerSpect models can not be directed used in machine learning models. This is due to the reason that their sizes vary dramatically during the filtration process. As seen in Fig 2, the number of 1-simplexes (edges) increases greatly during the filtration. In this way, the size of 1-D Hodge Laplacian matrixes and the number of related eigenvalues and eigenvectors will increase with the filtration. In our PerSpect models, a series of persistent attributes are considered [32]. The persistent attributes

are statistic and combinatorial properties of eigenvalues from the sequences of Hodge Laplacian matrices. They characterize the persistence and variation of spectral information during the filtration.

Here we can use eigenvalue-based Riemann Zeta functions. More specifically, for a set of eigenvalues  $\{\lambda_1, \lambda_2, \dots, \lambda_n\}$ , the Riemann Zeta functions are defined as,

$$\zeta(s) = \sum_{i=1}^n \frac{1}{\lambda_i^s}.$$

They can be used as molecular features for machine learning. In our model, we consider 11 types of different Riemann Zeta functions, i.e.,  $\zeta(s)$  with  $s = 5, 4, 3, 2, 1, 0, -1, -2, -3, -4, -5$ . Note that Riemann Zeta functions are related to different persistent spectral moments.

## DC-based machine learning models for protein-ligand binding affinity prediction

The prediction of protein-ligand binding affinity is arguably the most important step in virtual screening and AI-based drug design. Here we consider DC-based machine learning models. To characterize the detailed interactions between protein and ligand atoms, we consider element-specific bipartite graph representations. More specifically, we decompose the protein atoms at binding core regions into four groups according to their atoms types, including C, N, O, and S. Ligand atoms at binding core regions are decomposed into nine groups according to their atoms types, including C, N, O, S, P, F, Cl, Br, and I. In this way, there are totally  $36 = 4 \times 9$  groups of atom combinations, and protein-ligand interactions can be represented by 36 types of bipartite graphs from these atom combinations.

The bipartite graphs can be generated based on atom distances and electrostatic interactions. As stated above, the bipartite biadjacency matrix is represented as Eq (1). There are two different ways to define the weights. One is based on the Euclidian distance between atoms, that is  $w_{ij} = d(v_i, v_j)$  with  $d(v_i, v_j)$  the distance between atoms  $v_i$  and  $v_j$ . The other is based on atomic electrostatic interactions, that is  $w_{ij} = \frac{1}{1 + \exp\left(\frac{c q_i q_j}{d(v_i, v_j)}\right)}$  with  $q_i$  and  $q_j$  the partial charges of atoms  $v_i$  and  $v_j$  and parameter  $c$  a constant value (usually taken as 100). With the importance of hydrogen atom for electrostatic interactions, H atoms are usually taken into consideration and a total number of 50 types of atom combinations are considered for electrostatic interactions. The software ‘‘PDB2PQR’’ [45] is used to generate partial charge for protein while the partial charge of ligand can be found in PDBbind database.

We consider three most commonly-used datasets from PDBbind databank, including PDB-v2007, PDB-v2013 and PDB-v2016, as benchmark for our DC-based machine learning models. The detailed training and testing information are listed in Table 1. The binding core region is considered by using a cutoff distance of 10Å, that is all protein atoms within 10Å of any ligand atom. For distance-based DC models, the filtration goes from 2Å to 10Å with step 0.1Å, and for electrostatic-based DC models, the filtration goes from 0 to 1 with step 0.02. We only

**Table 1. Detailed information of the three PDBbind databases, i.e., PDBbind-v2007, PDBbind-v2013 and PDBbind-v2016.**

Dataset	Refined set	Training set	Test set (Core set)
PDBbind-v2007	1300	1105	195
PDBbind-v2013	2959	2764	195
PDBbind-v2016	4057	3772	285

<https://doi.org/10.1371/journal.pcbi.1009943.t001>

**Table 2. The parameters for our DC-based gradient boosting tree (GBT) models.**

No. of Estimators	Learning rate	Max depth	Subsample
40000	0.001	6	0.7
Min_samples_split	Loss function	Max features	Repetitions
2	Least square	SQRT	10

<https://doi.org/10.1371/journal.pcbi.1009943.t002>

consider 0-D persistent spectral information. In this way, the size of feature vectors are  $63360 = 36(\text{atom combinations}) \times 80(\text{filtration values}) \times 11(\text{Riemann Zeta functions}) \times 2(\text{two DCs})$ ,  $55000 = 50(\text{atom combinations}) \times 50(\text{filtration values}) \times 11(\text{Riemann Zeta functions}) \times 2(\text{two DCs})$  and  $118360 = 63360 + 55000$  for distance-based model, electrostatic-based model and combined model respectively. Gradient boosting tree is considered to alleviate the overfitting problem. The GBT setting is listed in Table 2.

**Scoring power.** The results for our DC-GBT models are listed in Table 3. Note that 10 independent regressions are performed and the median values of Pearson correlation coefficient (PCC) and root mean square error (RMSE) are taken as the final performance of our model. Further, we systematically compare our model with existing models with traditional learning descriptors [46–54]. Detailed comparison results can be found in Fig 3. It can be seen that our model outperforms all the other machine learning models with traditional molecular descriptors, for all three datasets.

Further, we compare our DC-GBT model with advanced-mathematical based machine learning models [14, 18, 20, 30]. The results are presented in Table 4. Our DC-GBT model is ranked as second for PDBbind-v2016 dataset and PDBbind-v2013 datasets (after TopBP). Note that the accuracy of our DC-based models can be further improved if convolutional neural network models, such as the one used in TopBP models, are designed and employed.

More recently, some deep learning models for protein-ligand binding affinity prediction are proposed, such as the graphDelta model [55], ECIF model [56], OnionNet-2 model [57], DeepAtom model [58] and others [54, 59–64]. Note that these new models usually employ a large training set with extra data from general sets from PDBbind. Details of the training sets, testing sets, and performance (PCC) of these models are listed in Table 5.

**Docking power.** We test the docking power, which is to identify the native poses from the ones generated by docking softwares [65], of our model on benchmark CASF-2013. There are totally 195 testing ligands in CASF-2013, each ligand has 100 poses generated from three docking programs, GOLD v5.1, Surflex-Dock in SYBYL v8.1 and MOE v2011. A pose is considered to be a native one if its RMSD value with respect to the true binding pose is less than 2 Å. Detailed RMSD information of all the ligands can be found in CASF-2013. If the pose with the highest predicted binding energy is a native one, it is regarded as a successful prediction. Once

**Table 3. The PCCs and RMSEs ( $pK_i/pK_i$ ) for our DC-GBT models in three test cases, i.e., PDBbind-v2007, PDBbind-v2013 and PDBbind-v2016.** Three DC-GBT models are considered with features from different types of bipartite graphs. The DC-GBT(Dist) model uses features from distance-based bipartite graphs; The DC-GBT(Chrg) model uses features from electrostatic-based bipartite graphs; The DC-GBT(Dist+Chrg) model uses features from both distance-based bipartite graphs and electrostatic-based bipartite graphs.

Dataset	Dist	Chrg	Dist+Chrg
PDBbind-v2007	0.816(1.416)	0.811(1.437)	0.824(1.402)
PDBbind-v2013	0.789(1.457)	0.790(1.456)	0.799(1.432)
PDBbind-v2016	0.836(1.270)	0.834(1.284)	0.843(1.255)
Average	0.813(1.377)	0.812(1.385)	0.822(1.357)

<https://doi.org/10.1371/journal.pcbi.1009943.t003>



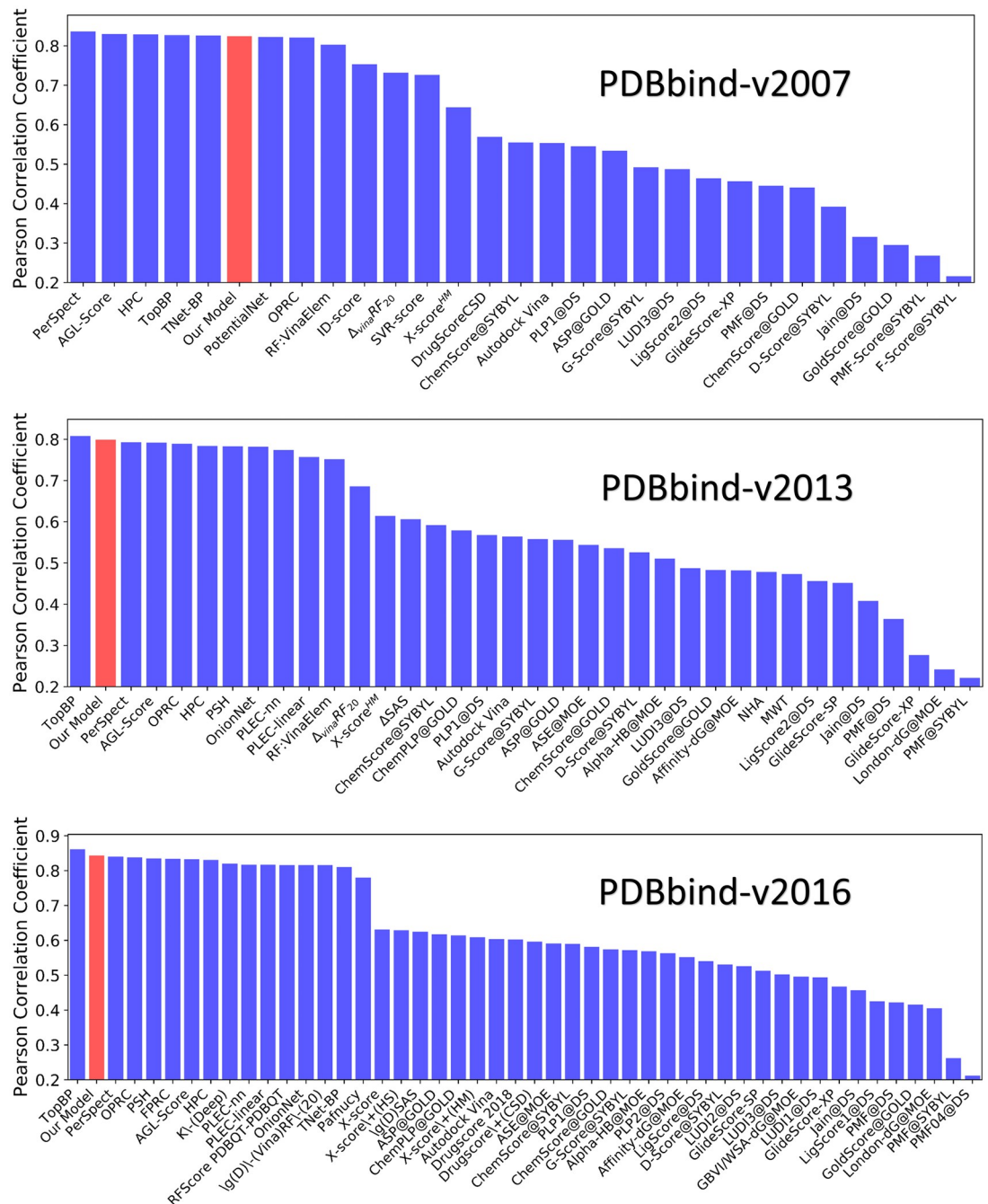


**Fig 3. Performance comparison between our models and other models.** The comparison of PCCs between our model and other molecular descriptor based models, for the prediction of protein-ligand binding affinity. The PCCs are calculated based on the core set (test set) of PDBbind-v2007, PDBbind-v2013 and PDBbind-v2016.

<https://doi.org/10.1371/journal.pcbi.1009943.g003>

this process is performed for the whole 195 testing ligands, an overall success rate can be computed for the given scoring function.

For each ligand, an individual training and testing process is needed. We repeat our DC-GBT(Dist) model for each of the 195 ligands, following the procedure in the work [18].

**Table 4. The comparison of our DC-GBT model with advanced-mathematical based machine learning models [14, 18, 20, 30, 32, 33].** Note that values marked with \* uses PDBbind-v2016 core set ( $N = 290$ ).

Model	PDBbind-v2007	PDBbind-v2013	PDBbind-v2016	Average
AGL-Score	0.830	0.792	0.833	0.818
HPC-GBT	0.829	0.784	0.831	0.815
TNet-BP	0.826	N/A	0.810*	N/A
TopBP	0.827	<b>0.808</b>	<b>0.861*</b>	<b>0.832</b>
PerSpect	<b>0.836</b>	0.793	0.840	0.823
OPRC	0.821	0.789	0.838	0.816
DC-GBT	0.824	0.799	0.843	0.822

<https://doi.org/10.1371/journal.pcbi.1009943.t004>

Note that GOLD v5.6.3 [66] is used to generate 1000 training poses for each ligand. These poses and their scores are available at <https://weilab.math.msu.edu/AGL-Score>.

In our implementation, ten independent regressions are performed for each ligand. The ligand is regarded as a successful one if at least three regressions successfully identify the native poses. In this case, our success rate can reach 88%. If we use at least six successful regressions as standard, our success rate drops slightly to 86%.

**Screening power.** The screening power of a scoring function is its ability to identify the true binders for a given target protein from decoy structures. We test our model on benchmark CASF-2013. There are totally 65 different proteins in CASF-2013. For each protein, there are at least three true binders while the rest of the 195 ligands are regarded as decoys. There are two kinds of screening power measurements. One is to find out the enrichment factors (EF) among the  $x\%$  top-ranked molecules.

$$EF_{x\%} = \frac{\text{number of true binders among } x\% \text{ top ranked molecules}}{(\text{total number of true binders for the given protein}) \times x\%}$$

where top-ranked molecules means the predicted candidates with high binding energies. And the average EF value among all 65 proteins is used to assess the screening power of a scoring function. The other is the success rate to identify the best true binders. For each target protein, if the the best binders are found in  $x\%$  top-ranked molecules, this protein is taken as a successful one. Then the overall success rate is given by the total number of successful proteins over 65.

For each protein, an individual training and testing process is considered. Our DC-GBT (Dist) model is used for each of 65 proteins, following the works [18]. More specifically, for a

**Table 5. The performance in terms of PCCs and RMSEs ( $pK_d/pK_i$ ) for recently-proposed models using different training sets [54–64].** Note that values marked with \* uses PDBbind-v2016 core set ( $N = 290$ ), and the values marked with + uses PDBbind-v2013 core set ( $N = 180$ ) and PDBbind-v2016 core set ( $N = 276$ ).

Model	Training set	Testing set1 core(PDB-v2013)	Testing set2 core(PDB-v2016)
graphDelta	PDB-v2018(8766)		0.87(1.05)
ECIF	PDB-v2019(9299)		0.866(1.169)
OnionNet-2	PDB-v2019(>9000)	0.821(1.357)	0.864(1.164)
DeepAtom	PDB-v2018(9383)		0.831(1.232)*
Ligand-based	PDB-v2018(11663)	0.780(N/A) <sup>+</sup>	0.821(N/A) <sup>+</sup>
SE-OnionNet	PDB-v2018(11663)	0.812(1.692)	0.83(N/A)
DeepDTAF	PDB-v2016(11906)		N/A(1.443)*
Deep Fusion	PDB-v2016(9226)		0.803(1.327*)

<https://doi.org/10.1371/journal.pcbi.1009943.t005>

given target protein, AutoDock Vina is used to dock all the ligands in PDBbind-v2015 refined set, excluding the core set and the true binders of this protein. This procedure gives rise to a few thousand of training poses and associated energy labels for each target protein. The binding scores (kcal/mol) generated by AutoDock Vina is converted to binding energy ( $pK_d$ ) by multiplying a constant -0.7335. Those binders in the refined set that do not bind to the target protein are regarded as decoys, and their binding energies should be smaller than the true binders. Therefore, if the energy of a decoy generated by AutoDock Vina is higher than the lower bound of the true binders' energies, the decoy is relabeled by the lower bound of the true binders' energies. Note that this procedure may cause many different decoys sharing same labels. The binding energy of a protein-ligand complex is usually a positive value, so we exclude the entries with negative binding energies from the training sets for all the 65 protein cases. The poses and associated scores can be found at <https://weilab.math.msu.edu/AGL-Score>.

In our implementation, for each protein, ten independent regressions are performed. As in PDBBind dataset, two decimal places are kept for the predicted binding energies of 195 testing ligands. For each regression, an EF value can be obtained and whether this protein is a successful one can be judged. The average EF value of ten regressions is taken as the final EF value for this protein in our model. Note that there are many different entries in the training set sharing the same labels, which results in that our model may predict same binding energies for different ligands. In this case, we take the first and second ranked ligands as the 1% top-ranked candidates. Hence the number of 1% top-ranked candidates maybe larger than 2. In this case, we set the EF to be 66.6. For the overall success rate, if at least two cases among the ten regressions assert that the given protein is a successful one, this protein is regarded as a successful one. In this case, our success rate can reach to 68%. If at least six successful regressions are used as standard, our success rate drops to about 58%.

Note that in our DC-GBT model, we consider target-specific scoring models and train them separately for scoring, docking and screening power tests. Previously, general scoring function models were developed. That is for all the tasks, the same general scoring function is used. Recently, data-driven learning models make use of the different types of training datasets to improve the performance of scoring functions. In particular, the incorporation of decoy data in the training set can significantly improve the docking and screening power [67–72]. In our DC-GBT models, different training sets are used, which results in different state-of-the-art scoring models in scoring, docking and screening power tests.

## Discussion

Machine learning models have made tremendous progresses in text, video, audio and image data analysis. In particular, convolutional neural network (CNN) models have achieved revolutionary advancements in the analysis of image data. However, molecular data from material, chemical and biological systems are fundamentally different from text and image data, as their properties are usually directly determined by their topological structures. Persistent models, including persistent homology/cohomology, persistent functions, and persistent spectral, provide a series of highly effective molecular descriptors that not only preserve intrinsic structural information, but also maintain molecular multiscale properties. Here we propose Dowker complex based machine learning models for drug design. Dowker complex is used for molecular interaction representation. Riemann Zeta functions are defined on persistent spectral models and further used as molecular descriptors. Our Dowker complex based machine learning models have achieved state-of-the-art results for protein-ligand binding affinity. They can be also be used in AI-based drug design and other molecular data analysis.

## Materials and methods

Our model contains two essential components, i.e., DC-based molecular representation and DC-based PerSpect models. For a molecular interaction-based bipartite graph, its associated DCs can be decomposed into two disjoint DCs which have the same homology groups. The DC-based Hodge-Laplacian matrices and Riemann Zeta function can be constructed and further used in the generation of molecular features for machine learning models.

### DC-based persistent homology

Dowker complex is based on the “relations” of two sets and is originally developed to explore the homology of relations [38]. Mathematically, a relation is equivalent to a bipartite graph. So for each bipartite graph, a Dowker complex can be naturally constructed. More specifically, let  $G$  be a bipartite graph, the DC  $K_D(G)$  will have two disjoint components  $K_{D,1}(G)$  and  $K_{D,2}(G)$ . Assume  $G = (V_1, V_2, E)$  is a connected bipartite graph where  $V_1$  and  $V_2$  are two vertex sets and  $E$  is the edge set that form only between  $V_1$  and  $V_2$ .  $K_D(G) = K_{D,1}(G) \cup K_{D,2}(G)$  where  $K_{D,1}(G)$  and  $K_{D,2}(G)$  are the two disjoint components of  $K_D(G)$ ,  $K_{D,1}(G)$  and  $K_{D,2}(G)$  are defined as follows:

- $K_{D,1}(G)$ : for a set of vertices  $\{x_{i_0}, x_{i_1}, \dots, x_{i_p}\}$  in  $V_1$ , a  $p$ -simplex is formed among these vertices in  $K_{D,1}(G)$ , if there exists a vertex  $y \in V_2$  such that  $\{(x_{i_m}, y) | 0 \leq m \leq p\} \subset E$ .
- $K_{D,2}(G)$ : for a set of vertices  $\{y_{i_0}, y_{i_1}, \dots, y_{i_p}\}$  in  $V_2$ , a  $p$ -simplex is formed among these vertices in  $K_{D,2}(G)$ , if there exists a vertex  $x \in V_1$  such that  $\{(x, y_{i_m}) | 0 \leq m \leq p\} \subset E$ .

An example can be found in Fig 4. It can be seen that the Dowker complex just has two disjoint components, one is in black points and the other is in green points, and a simplex is formed if their vertices have a common neighbor vertex in the bipartite graph. Like the triangle in black points, its three vertices has a common green point as neighbor vertex in the bipartite graph. We have  $H_p(K_{D,1}(G)) \cong H_p(K_{D,2}(G)) (0 \leq p)$ . Actually  $K_{D,1}(G)$  and  $K_{D,2}(G)$  are homotopic equivalent.

Finally, if we construct the bipartite graph filtration process as in Eq (2), and induce the DC-based filtration as in Eq (3). Two separated DC sequences are generated as Eqs (4) and (5). The corresponding persistent barcodes of these two DC sequences are exactly same.

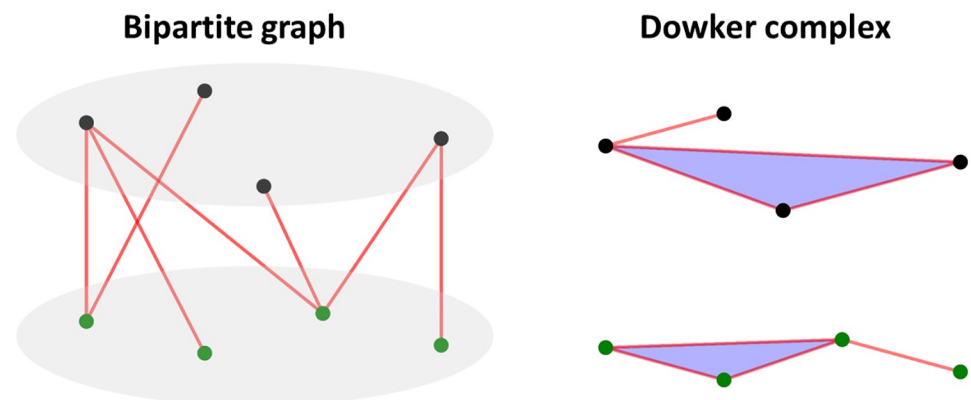


**Fig 4. A bipartite graph and its associated Dowker complex.** It can be seen that there are two disjoint components in DC, one is from the black points and the other is from the green points. Note that a triangle (2-simplex) is formed among the black point set in DC, as the corresponding three black vertices have a common neighbor blue vertex in the bipartite graph.

<https://doi.org/10.1371/journal.pcbi.1009943.g004>

### DC-based PerSpect models

Persistent spectral theory studies the spectral evolutionary information of combinatorial Laplacian matrixes associated with a filtration process. An oriented DC is needed for the construction of combinatorial Laplacian matrixes, but different orientations share the same eigen spectral information. In this way, we can define an orientation based on the sequence of atoms (as in PDB file) for simplicity.

For an oriented DC  $K_D = \{\delta_k^i; k = 0, 1, \dots; i = 1, 2, \dots\}$ , its  $k$ -th boundary matrix  $B_k$  can be defined as follows,

$$B_k(i, j) = \begin{cases} 1, & \text{if } \delta_i^{k-1} \subset \delta_j^k \text{ and } \delta_i^{k-1} \sim \delta_j^k \\ -1, & \text{if } \delta_i^{k-1} \subset \delta_j^k \text{ and } \delta_i^{k-1} \not\sim \delta_j^k \\ 0, & \text{if } \delta_i^{k-1} \not\subset \delta_j^k. \end{cases}$$

Here  $\delta_i^{k-1} \subset \delta_j^k$  means that  $\delta_i^{k-1}$  is a face of  $\delta_j^k$  and  $\delta_i^{k-1} \not\subset \delta_j^k$  means the opposite. The notation  $\delta_i^{k-1} \sim \delta_j^k$  means the two simplexes have the same orientation, i.e., oriented similarly, and  $\delta_i^{k-1} \not\sim \delta_j^k$  means the opposite.

The  $k$ -th laplacian matrix is defined as follows,

$$L_k = B_k^T B_k + B_{k+1} B_{k+1}^T.$$

More specifically,  $L_0$  can be expressed explicitly as,

$$L_0(i, j) = \begin{cases} d(\delta_i^0), & \text{if } i = j \\ -1, & \text{if } i \neq j, \delta_i^0 \sim \delta_j^0, \\ 0, & \text{if } i \neq j, \delta_i^0 \not\sim \delta_j^0 \end{cases} \tag{8}$$

Further,  $L_k(k > 0)$  can be expressed as,

$$L_k(i, j) = \begin{cases} d(\delta_i^k) + k + 1, & \text{if } i = j \\ 1, & \text{if } i \neq j, \delta_i^k \not\sim \delta_j^k, \delta_i^k \sim \delta_j^k \text{ and } \delta_i^k \sim \delta_j^k \\ -1, & \text{if } i \neq j, \delta_i^k \not\sim \delta_j^k, \delta_i^k \sim \delta_j^k \text{ and } \delta_i^k \not\sim \delta_j^k \\ 0, & \text{if } i \neq j, \delta_i^k \sim \delta_j^k \text{ or } \delta_i^k \not\sim \delta_j^k. \end{cases}$$

Here  $d(\delta_i^k)$  is (upper) degree of  $k$ -simplex  $\delta_i^k$ . It is the number of  $(k + 1)$ -simplexes, of which  $\delta_i^k$  is a face. Notation  $\delta_i^k \sim \delta_j^k$  means the two simplexes are upper adjacent, i.e., they are faces of a common  $(k + 1)$ -simplex, and  $\delta_i^k \not\sim \delta_j^k$  means the opposite. Notation  $\delta_i^k \sim \delta_j^k$  means the two simplexes are lower adjacent, i.e., they share a common  $(k - 1)$ -simplex as their face, and  $\delta_i^k \not\sim \delta_j^k$  means the opposite. Notation  $\delta_i^k \sim \delta_j^k$  means the two simplexes have the same orientation, i.e., oriented similarly, and  $\delta_i^k \not\sim \delta_j^k$  means the opposite.

In our model, we consider the Riemann Zeta functions on the spectral as our persistent attributes. More specifically, for a set of eigenvalues  $\{\lambda_1, \lambda_2, \dots, \lambda_n\}$ , the spectral moment of the simplicial complex can be defined as the Zeta function  $\zeta(s) = \sum_{i=1}^n \frac{1}{\lambda_i^s}$ . Then we use the persistent spectral moment as the persistent attributes for machine learning.



## Author Contributions

**Conceptualization:** Kelin Xia.

**Data curation:** Xiang Liu, Kelin Xia.

**Formal analysis:** Xiang Liu, Kelin Xia.

**Funding acquisition:** Kelin Xia.

**Investigation:** Kelin Xia.

**Methodology:** Xiang Liu, Kelin Xia.

**Project administration:** Kelin Xia.

**Resources:** Huitao Feng, Jie Wu, Kelin Xia.

**Supervision:** Kelin Xia.

**Validation:** Xiang Liu, Kelin Xia.

**Visualization:** Xiang Liu.

**Writing – original draft:** Kelin Xia.

**Writing – review & editing:** Xiang Liu, Huitao Feng, Jie Wu, Kelin Xia.

## References

1. Puzyn T, Leszczynski J, Cronin MT. Recent advances in QSAR studies: methods and applications. vol. 8. Springer Science & Business Media; 2010.
2. Lo YC, Rensi SE, Torng W, Altman RB. Machine learning in chemoinformatics and drug discovery. *Drug discovery today*. 2018; 23(8):1538–1546. <https://doi.org/10.1016/j.drudis.2018.05.010> PMID: 29750902
3. Durant JL, Leland BA, Henry DR, Nourse JG. Reoptimization of MDL keys for use in drug discovery. *Journal of chemical information and computer sciences*. 2002; 42(6):1273–1280. <https://doi.org/10.1021/ci010132r> PMID: 12444722
4. O'Boyle NM, Banck M, James CA, Morley C, Vandermeersch T, Hutchison GR. Open Babel: An open chemical toolbox. *Journal of cheminformatics*. 2011; 3(1):33. <https://doi.org/10.1186/1758-2946-3-33> PMID: 21982300
5. Hall LH, Kier LB. Electrotopological state indices for atom types: a novel combination of electronic, topological, and valence state information. *Journal of Chemical Information and Computer Sciences*. 1995; 35(6):1039–1045. <https://doi.org/10.1021/ci00028a014>
6. Rogers D, Hahn M. Extended-connectivity fingerprints. *Journal of chemical information and modeling*. 2010; 50(5):742–754. <https://doi.org/10.1021/ci100050t> PMID: 20426451
7. Landrum G. RDKit: Open-source cheminformatics. 2006;.
8. Stiefl N, Watson IA, Baumann K, Zaliani A. ErG: 2D pharmacophore descriptions for scaffold hopping. *Journal of chemical information and modeling*. 2006; 46(1):208–220. <https://doi.org/10.1021/ci050457y> PMID: 16426057
9. Merkwirth C, Lengauer T. Automatic generation of complementary descriptors with molecular graph networks. *Journal of chemical information and modeling*. 2005; 45(5):1159–1168. <https://doi.org/10.1021/ci049613b> PMID: 16180893
10. Duvenaud DK, Maclaurin D, Iparraguirre J, Bombarell R, Hirzel T, Aspuru-Guzik A, et al. Convolutional networks on graphs for learning molecular fingerprints. In: *Advances in neural information processing systems*; 2015. p. 2224–2232.
11. Coley CW, Barzilay R, Green WH, Jaakkola TS, Jensen KF. Convolutional embedding of attributed molecular graphs for physical property prediction. *Journal of chemical information and modeling*. 2017; 57(8):1757–1772. <https://doi.org/10.1021/acs.jcim.6b00601> PMID: 28696688
12. Xu Y, Pei J, Lai L. Deep learning based regression and multiclass models for acute oral toxicity prediction with automatic chemical feature extraction. *Journal of chemical information and modeling*. 2017; 57(11):2672–2685. <https://doi.org/10.1021/acs.jcim.7b00244> PMID: 29019671

13. Winter R, Montanari F, Noé F, Clevert DA. Learning continuous and data-driven molecular descriptors by translating equivalent chemical representations. *Chemical science*. 2019; 10(6):1692–1701. <https://doi.org/10.1039/c8sc04175j> PMID: 30842833
14. Cang ZX, Wei GW. TopologyNet: Topology based deep convolutional and multi-task neural networks for biomolecular property predictions. *PLOS Computational Biology*. 2017; 13(7):e1005690. <https://doi.org/10.1371/journal.pcbi.1005690> PMID: 28749969
15. Cang ZX, Wei GW. Integration of element specific persistent homology and machine learning for protein-ligand binding affinity prediction. *International journal for numerical methods in biomedical engineering*. 2017;. PMID: 28677268
16. Nguyen DD, Xiao T, Wang ML, Wei GW. Rigidity Strengthening: A Mechanism for Protein–Ligand Binding. *Journal of chemical information and modeling*. 2017; 57(7):1715–1721. <https://doi.org/10.1021/acs.jcim.7b00226> PMID: 28665130
17. Cang ZX, Wei GW. Integration of element specific persistent homology and machine learning for protein-ligand binding affinity prediction. *International journal for numerical methods in biomedical engineering*. 2018; 34(2):e2914. <https://doi.org/10.1002/cnm.2914> PMID: 28677268
18. Nguyen DD, Wei GW. AGL-Score: Algebraic Graph Learning Score for Protein-Ligand Binding Scoring, Ranking, Docking, and Screening. *Journal of chemical information and modeling*. 2019; 59(7):3291–3304. <https://doi.org/10.1021/acs.jcim.9b00334> PMID: 31257871
19. Cang ZX, Wei GW. Analysis and prediction of protein folding energy changes upon mutation by element specific persistent homology. *Bioinformatics*. 2017; 33(22):3549–3557. PMID: 29036440
20. Cang ZX, Mu L, Wei GW. Representability of algebraic topology for biomolecules in machine learning based scoring and virtual screening. *PLoS computational biology*. 2018; 14(1):e1005929. <https://doi.org/10.1371/journal.pcbi.1005929> PMID: 29309403
21. Wu KD, Wei GW. Quantitative toxicity prediction using topology based multi-task deep neural networks. *Journal of chemical information and modeling*. 2018;. <https://doi.org/10.1021/acs.jcim.7b00558>
22. Wang B, Zhao ZX, Wei GW. Automatic parametrization of non-polar implicit solvent models for the blind prediction of solvation free energies. *The Journal of chemical physics*. 2016; 145(12):124110. <https://doi.org/10.1063/1.4963193> PMID: 27782659
23. Wang B, Wang CZ, Wu KD, Wei GW. Breaking the polar-nonpolar division in solvation free energy prediction. *Journal of computational chemistry*. 2018; 39(4):217–233. <https://doi.org/10.1002/jcc.25107> PMID: 29127720
24. Wu KD, Zhao ZX, Wang RX, Wei GW. TopP–S: Persistent homology-based multi-task deep neural networks for simultaneous predictions of partition coefficient and aqueous solubility. *Journal of computational chemistry*. 2018; 39(20):1444–1454. <https://doi.org/10.1002/jcc.25213> PMID: 29633287
25. Zhao RD, Cang ZX, Tong YY, Wei GW. Protein pocket detection via convex hull surface evolution and associated Reeb graph. *Bioinformatics*. 2018; 34(17):i830–i837. <https://doi.org/10.1093/bioinformatics/bty598> PMID: 30423105
26. Grow C, Gao KF, Nguyen DD, Wei GW. Generative network complex (GNC) for drug discovery. *arXiv preprint arXiv:191014650*. 2019;.
27. Nguyen DD, Cang ZX, Wu KD, Wang ML, Cao Y, Wei GW. Mathematical deep learning for pose and binding affinity prediction and ranking in D3R Grand Challenges. *Journal of computer-aided molecular design*. 2019; 33(1):71–82. <https://doi.org/10.1007/s10822-018-0146-6> PMID: 30116918
28. Nguyen DD, Gao KF, Wang ML, Wei GW. MathDL: Mathematical deep learning for D3R Grand Challenge 4. *Journal of computer-aided molecular design*. 2019; p. 1–17. <https://doi.org/10.1007/s10822-019-00237-5> PMID: 31734815
29. Nguyen DD, Cang ZX, Wu KD, Wang ML, Cao Y, Wei GW. Mathematical deep learning for pose and binding affinity prediction and ranking in D3R Grand Challenges. *Journal of computer-aided molecular design*. 2019; 33(1):71–82. <https://doi.org/10.1007/s10822-018-0146-6> PMID: 30116918
30. Liu X, J WX, Wu J, Xia KL. Hypergraph based persistent cohomology (HPC) for molecular representations in drug design. *Briefings in Bioinformatics*. 2021;. PMID: 33480394
31. Liu X, Feng H, Wu J, Xia K. Persistent spectral hypergraph based machine learning (PSH-ML) for protein-ligand binding affinity prediction. *Briefings in Bioinformatics*;. PMID: 33837771
32. Meng ZY, Xia KL. Persistent spectral based machine learning (PerSpect ML) for drug design. *Science Advances*, 2021;. <https://doi.org/10.1126/sciadv.abc5329>
33. Wee J, Xia K. Ollivier Persistent Ricci Curvature-Based Machine Learning for the Protein–Ligand Binding Affinity Prediction. *Journal of Chemical Information and Modeling*;. PMID: 33724038
34. Wee J, Xia K. Forman persistent Ricci curvature (FPRC) based machine learning models for protein-ligand binding affinity prediction. *Briefings in Bioinformatics*, 2021;. <https://doi.org/10.1093/bib/bbab136> PMID: 33940588

35. Wang R, Nguyen DD, Wei GW. Persistent spectral graph. *International Journal for Numerical Methods in Biomedical Engineering*. 2020; p. e3376. <https://doi.org/10.1002/cnm.3376> PMID: 32515170
36. Wang R, Zhao R, Ribando-Gros E, Chen J, Tong Y, Wei GW. HERMES: Persistent spectral graph software. *Foundations of Data Science*. 2020; 3:67–97. <https://doi.org/10.3934/fods.2021006>
37. Björner A. Topological methods. *Handbook of combinatorics*. 1995; 2:1819–1872.
38. Dowker CH. Homology groups of relations. *Annals of mathematics*. 1952; p. 84–95. <https://doi.org/10.2307/1969768>
39. Chowdhury S, Mémoli F. A functorial Dowker theorem and persistent homology of asymmetric networks. *Journal of Applied and Computational Topology*. 2018; 2(1):115–175. <https://doi.org/10.1007/s41468-018-0020-6>
40. Nguyen DD, Cang ZX, Wei GW. A review of mathematical representations of biomolecular data. *Physical Chemistry Chemical Physics*. 2020;. <https://doi.org/10.1039/c9cp06554g> PMID: 32067019
41. Gao K, Nguyen DD, Sresht V, Mathiowetz AM, Tu M, Wei GW. Are 2D fingerprints still valuable for drug discovery? *Physical chemistry chemical physics*. 2020; 22(16):8373–8390. <https://doi.org/10.1039/d0cp00305k> PMID: 32266895
42. Nguyen DD, Gao K, Wang M, Wei GW. MathDL: mathematical deep learning for D3R Grand Challenge 4. *Journal of computer-aided molecular design*. 2020; 34(2):131–147. <https://doi.org/10.1007/s10822-019-00237-5> PMID: 31734815
43. Zhou T, Ren J, Medo M, Zhang YC. Bipartite network projection and personal recommendation. *Physical review E*. 2007; 76(4):046115. <https://doi.org/10.1103/PhysRevE.76.046115> PMID: 17995068
44. Pavlopoulos GA, Kontou PI, Pavlopoulou A, Bouyioukos C, Markou E, Bagos PG. Bipartite graphs in systems biology and medicine: a survey of methods and applications. *GigaScience*. 2018; 7(4):giy014. <https://doi.org/10.1093/gigascience/giy014>
45. Dolinsky TJ, Czodrowski P, Li H, Nielsen JE, Jensen JH, Klebe G, et al. PDB2PQR: Expanding and upgrading automated preparation of biomolecular structures for molecular simulations. *Nucleic Acids Res*. 2007; 35:W522–525. <https://doi.org/10.1093/nar/gkm276> PMID: 17488841
46. Liu J, Wang RX. Classification of current scoring functions. *Journal of chemical information and modeling*. 2015; 55(3):475–482. <https://doi.org/10.1021/ci500731a> PMID: 25647463
47. Li HJ, Leung KS, Wong MH, Ballester PJ. Improving AutoDock Vina using random forest: the growing accuracy of binding affinity prediction by the effective exploitation of larger data sets. *Molecular informatics*. 2015; 34(2-3):115–126. <https://doi.org/10.1002/minf.201400132> PMID: 27490034
48. Wójcikowski M, Kukielka M, Stepniewska-Dziubinska MM, Siedlecki P. Development of a protein–ligand extended connectivity (PLEC) fingerprint and its application for binding affinity predictions. *Bioinformatics*. 2019; 35(8):1334–1341. <https://doi.org/10.1093/bioinformatics/bty757> PMID: 30202917
49. Jiménez J, Skalic M, Martínez-Rosell G, De Fabritiis G.  $K_{DEEP}$ . Protein–ligand absolute binding affinity prediction via 3D-convolutional neural networks. *Journal of chemical information and modeling*. 2018; 58(2):287–296. <https://doi.org/10.1021/acs.jcim.7b00650> PMID: 29309725
50. Stepniewska-Dziubinska MM, Zielenkiewicz P, Siedlecki P. Development and evaluation of a deep learning model for protein–ligand binding affinity prediction. *Bioinformatics*. 2018; 34(21):3666–3674. <https://doi.org/10.1093/bioinformatics/bty374> PMID: 29757353
51. Su MY, Yang QF, Du Y, Feng GQ, Liu ZH, Li Y, et al. Comparative assessment of scoring functions: The CASF-2016 update. *Journal of chemical information and modeling*. 2018; 59(2):895–913. <https://doi.org/10.1021/acs.jcim.8b00545> PMID: 30481020
52. Afifi K, Al-Sadek AF. Improving classical scoring functions using random forest: The non-additivity of free energy terms' contributions in binding. *Chemical biology & drug design*. 2018; 92(2):1429–1434. <https://doi.org/10.1111/cbdd.13206> PMID: 29655201
53. Feinberg EN, Sur D, Wu ZQ, Husic BE, Mai HH, Li Y, et al. PotentialNet for molecular property prediction. *ACS central science*. 2018; 4(11):1520–1530. <https://doi.org/10.1021/acscentsci.8b00507> PMID: 30555904
54. Boyles F, Deane CM, Morris GM. Learning from the ligand: using ligand-based features to improve binding affinity prediction. *Bioinformatics*. 2020; 36(3):758–764. PMID: 31598630
55. Karlov DS, Sosnin S, Fedorov MV, Popov P. graphDelta: MPNN scoring function for the affinity prediction of protein–ligand complexes. *ACS omega*. 2020; 5(10):5150–5159. <https://doi.org/10.1021/acsomega.9b04162> PMID: 32201802
56. Sánchez-Cruz N, Medina-Franco JL, Mestres J, Barril X. Extended connectivity interaction features: Improving binding affinity prediction through chemical description. *Bioinformatics*. 2021; 37(10):1376–1382. <https://doi.org/10.1093/bioinformatics/btaa982> PMID: 33226061

57. Wang Z, Zheng L, Liu Y, Qu Y, Li YQ, Zhao M, et al. OnionNet-2: A Convolutional Neural Network Model for Predicting Protein-Ligand Binding Affinity based on Residue-Atom Contacting Shells. arXiv preprint arXiv:210311664. 2021;.
58. Rezaei MA, Li Y, Wu DO, Li X, Li C. Deep Learning in Drug Design: Protein-Ligand Binding Affinity Prediction. *IEEE/ACM Transactions on Computational Biology and Bioinformatics*. 2020;.
59. Song T, Wang S, Liu D, Ding M, Du Z, Zhong Y, et al. SE-OnionNet: A convolution neural network for protein-ligand binding affinity prediction. *Frontiers in Genetics*. 2020; 11:1805. <https://doi.org/10.3389/fgene.2020.607824> PMID: 33737946
60. Zhu F, Zhang X, Allen JE, Jones D, Lightstone FC. Binding Affinity Prediction by Pairwise Function Based on Neural Network. *Journal of chemical information and modeling*. 2020; 60(6):2766–2772. <https://doi.org/10.1021/acs.jcim.0c00026> PMID: 32338892
61. Wang K, Zhou R, Li Y, Li M. DeepDTAF: a deep learning method to predict protein–ligand binding affinity. *Briefings in Bioinformatics*. 2021; . PMID: 33834190
62. Zhou J, Li S, Huang L, Xiong H, Wang F, Xu T, et al. Distance-aware Molecule Graph Attention Network for Drug-Target Binding Affinity Prediction. arXiv preprint arXiv:201209624. 2020;.
63. Jones D, Kim H, Zhang X, Zemla A, Stevenson G, Bennett WD, et al. Improved Protein–Ligand Binding Affinity Prediction with Structure-Based Deep Fusion Inference. *Journal of Chemical Information and Modeling*. 2021; 61(4):1583–1592. <https://doi.org/10.1021/acs.jcim.0c01306> PMID: 33754707
64. Hassan-Harrirou H, Zhang C, Lemmin T. RosENet: Improving Binding Affinity Prediction by Leveraging Molecular Mechanics Energies with an Ensemble of 3D Convolutional Neural Networks. *Journal of Chemical Information and Modeling*. 2020;. <https://doi.org/10.1021/acs.jcim.0c00075> PMID: 32392050
65. Cheng T, Li X, Li Y, Liu Z, Wang R. Comparative assessment of scoring functions on a diverse test set. *Journal of chemical information and modeling*. 2009; 49(4):1079–1093. <https://doi.org/10.1021/ci9000053> PMID: 19358517
66. Jones G, Willett P, Glen RC, Leach AR, Taylor R. Development and validation of a genetic algorithm for flexible docking. *Journal of molecular biology*. 1997; 267(3):727–748. <https://doi.org/10.1006/jmbi.1996.0897> PMID: 9126849
67. Pham TA, Jain AN. Parameter estimation for scoring protein- ligand interactions using negative training data. *Journal of medicinal chemistry*. 2006; 49(20):5856–5868. <https://doi.org/10.1021/jm050040j> PMID: 17004701
68. Durrant JD, McCammon JA. NNScore: a neural-network-based scoring function for the characterization of protein- ligand complexes. *Journal of chemical information and modeling*. 2010; 50(10):1865–1871. <https://doi.org/10.1021/ci100244v> PMID: 20845954
69. Li L, Wang B, Meroueh SO. Support vector regression scoring of receptor–ligand complexes for rank-ordering and virtual screening of chemical libraries. *Journal of chemical information and modeling*. 2011; 51(9):2132–2138. <https://doi.org/10.1021/ci200078f> PMID: 21728360
70. Ragoza M, Hochuli J, Idrobo E, Sunseri J, Koes DR. Protein–ligand scoring with convolutional neural networks. *Journal of chemical information and modeling*. 2017; 57(4):942–957. <https://doi.org/10.1021/acs.jcim.6b00740> PMID: 28368587
71. Wang C, Zhang Y. Improving scoring-docking-screening powers of protein–ligand scoring functions using random forest. *Journal of computational chemistry*. 2017; 38(3):169–177. <https://doi.org/10.1002/jcc.24667> PMID: 27859414
72. Bao J, He X, Zhang JZ. DeepBSP—a machine learning method for accurate prediction of protein–ligand docking structures. *Journal of Chemical Information and Modeling*. 2021; 61(5):2231–2240. <https://doi.org/10.1021/acs.jcim.1c00334> PMID: 33979150